JJEES

Volume 2, (Special Publication, Number 1), December. 2009
ISSN 1995-6681
Pages 96- 107

Jordan Journal of Earth and Environmental Sciences

Determination of crystallite thickness and crystal growth mechanisms of Jordanian clays by X-ray diffraction method.

I.M.Odeh [a], W.A.Saqqa [b], D.Eberl [c]

[a] Department of Physics, Yarmouk University, Irbid, Jordan,

[b] Department of Earth & Environmental Sciences,Yarmouk University, Irbid, Jordan

[c] U.S. Geological Survey, 3215 Marine St., Boulder, CO 80303-1066 USA

Abstract

Five mudrock samples were collected at different stratigraphical positions within the rock column of Jordan. They represent the ages of the late Ordovician-lower Silurian (SIL sample), late Permian (UI sample), Lower Cretaceous (MAH sample), Lower Turonian (TAF sample) and Pleistocene (YAM sample). The results of X-ray diffraction (XRD) analysis of clay fraction (particle size < 2 μm) show that the amount of smectite decreases towards more ancient mudrock samples, i.e. towards an increase of burial depth. Smectite totally disappeared in the Silurian claystone (SIL sample) at a depth of 1.6 km more likely as a function of burial diagenesis. The change of smectite into illite, due to burial history, was through a mixed layer illite-smectite intermediate stage of alteration. The shape of crystallite thickness distributions (CTDs) for illite was asymptotic in all study samples. This means that the crystal growth mechanism of illite particles was similar regardless of the burial depth of sediments and was concurrent with nucleation. The XRD patterns showed that the degree of Kaolinite crystallinity increased generally with depth as the 001 reflection becomes sharper and narrower. The CTDs shapes for kaolinite were somewhat different. It was asymptotic in YAM and TAF samples, multimodal in MAH sample, and lognormal in UI and SIL samples. These variations in CTDs distributions reflect the fact that crystal growth mechanism of kaolinite differed with burial depth. Kaolinite crystal growth accompanied with nucleation was only at shallow-moderate depths. This changed to crystal growth without continued nucleation at greater depths.

Keywords :X-ray diffraction, Jordanian clays, MudMaster Program, crystallite thickness distribution, asymptotic shape, lognormal shape.

1. Introduction

The use of X-ray diffraction (XRD) to study the crystallinity of clay minerals, crystallites sizes and the shapes of crystallite thickness distributions (CTDs) have attracted considerable attention over the past years. Dudek et al. (2002) pointed to several mathematical approaches in order to obtain information about crystal size from the XRD peak shapes. Of these approaches is Scherer equation (Drits et al., 1997), variance method (Wilson, 1963 in Árkai et al., 1996), Bertaut-Warren-Averbach (BWA) method (Eberl et al., 1996; Drits et al., 1998). While Scherrer's equation yields the mean crystallite thickness, variance and Voigt methods give information regarding the mean size and strain (Dudek et al., 2002). The BWA-method however, is most universal because it is capable of measuring the crystallite mean size, strain and crystallites size distributions. The latter method forms the basis of a computer program known as MudMaster, which was produced by Eberl et al. (1996) and later developed by Drits et al., (1998). MudMaster is capable of determining the particle size, crystallites size distributions and strain for different types of clay minerals such as Illite, kaolinite, smectite, and some other clay minerals. Determination of crystallites thicknesses of illite by either XRD or TEM (Eberl and Velde, 1989; Merriman et al., 1990; Nieto and Sánchez-Navaz, 1994; Lanson et al., 1996; Arkai et al., 1996; Eberl et al., 1996; 1998a, b; Drits et al., 1998; Jaboyedoff et al., 2001; Brime and Eberl, 2002) is as an alternative approach for methods based on measuring illite crystallinity by determining the Kübler index. The evolution of illite in mudrock during burial diagenesis was better explained by applying the BWA-method (Brume and Eberl, 2002). According to the later authors and earlier to (Eberl et al., 1996) the resulting crystallite thickness distributions (CTDs) exhibit asymptotic, lognormal and multimodal shapes. These CTD's can suggest information about nucleation, crystal growth mechanism, and history based on the theoretical approach of Eberl et al. (1998a). The resulting shapes can be used to establish a model for crystal growth of clay minerals.

The present study employed the X-ray diffraction and the MudMaster software for measuring the mean crystallite thickness, crystallite thickness distributions (CTDs) of illite and kaolinite in some selected Paleozoic-Pleistocene Jordanian mudrock samples. These measurements aim to determine changes in crystallite size,

* Corresponding author. iodeh@yu.edu.jo

the mean crystallite thickness and the CTDs shapes of illite (I) and kaolinite (K) and to detect their crystal growth mechanisms from measurements of the *001* basal reflections

2. Materials

Five mudrock samples were selected for this study (Fig. 1).

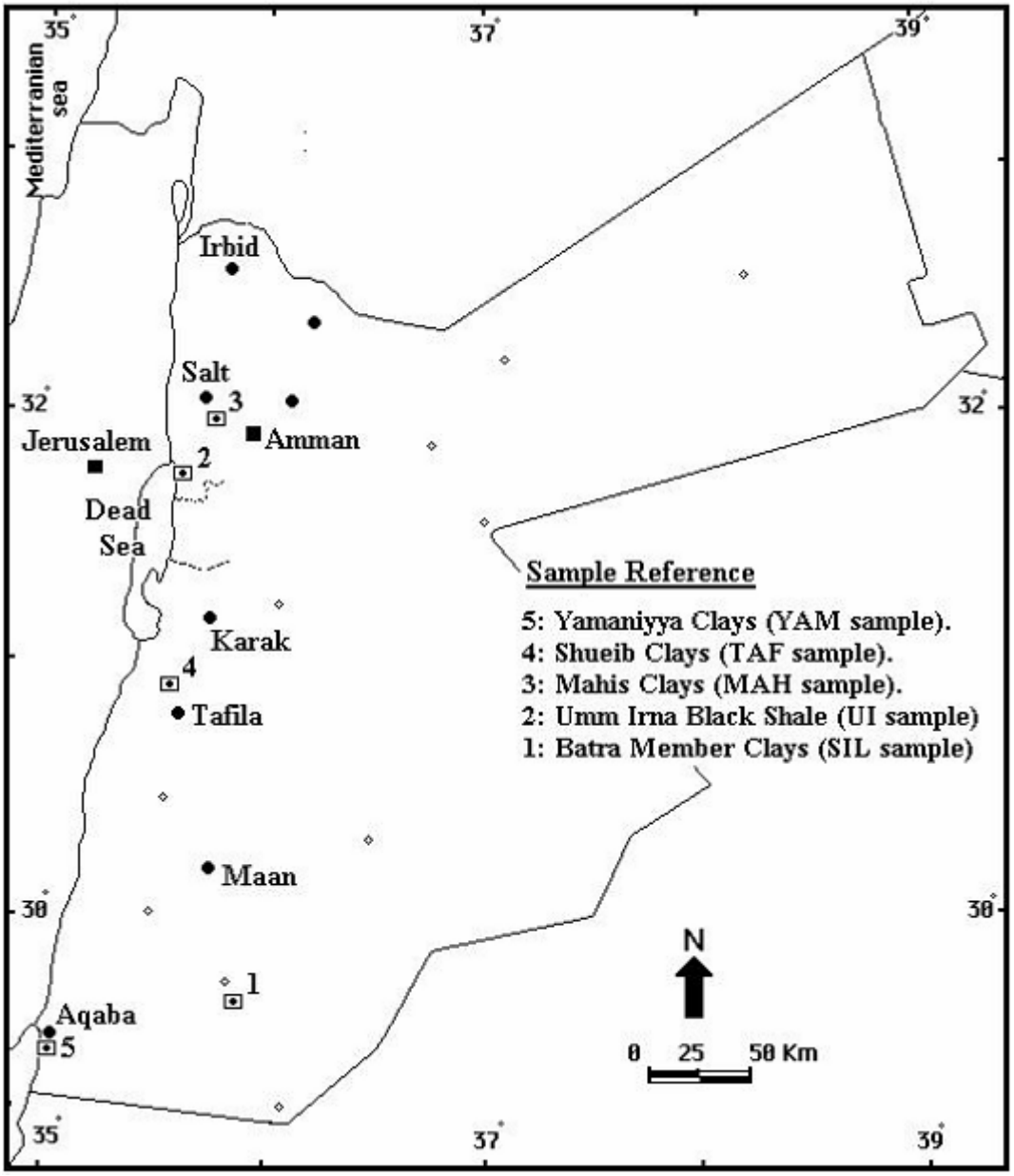

Fig(1). Locations of study samples.

The first and most ancient sample (Sample Ref., SIL) refers to the late Ordovician-early Silurian Batra Member grayish-green kaolinitic clay stone with an abundance of Graptolite remains found at bedding planes. Clay stones are interbedded with reddish siltstone-fine sandstone beds (Fig. 2). Batra Member is about 80 m thick and of marine origin (Abed, 2000). The second sample (Sample Ref., UIR) was selected from the black shale horizons with plant remains in the upper parts of the late Permian Umm Irna Formation cropping out close to the northeastern Dead Sea shorelines. The formation consists principally of two quartz arenite sandstone facies (60 m. thick) with fining upward cycles. Each starts with pebbly sandstone at the base and changes upward into fine sandstone, siltstone and silty clay stone (Fig.2). The uppermost two cycles are distinguished by the presence of reddish-brown and occasionally dark gray paleosol horizons separated from each other by the dark gray-black shale beds (Makhlouf et al., 1991) from which UIR sample was collected. The third sample (Sample Ref., MAH) was selected from the light gray-green kaolinitic clay deposits interbedding a thick sandstone sequence (≅ 200m) of the Lower Cretaceous Kurnub Group, which crops out in Mahis area (Fig. 2). The fourth sample (Sample Ref., TAF) was selected from the Turonian Shueib Formation. This formation crops out in the area between Karak and Tafila, south of Jordan. The

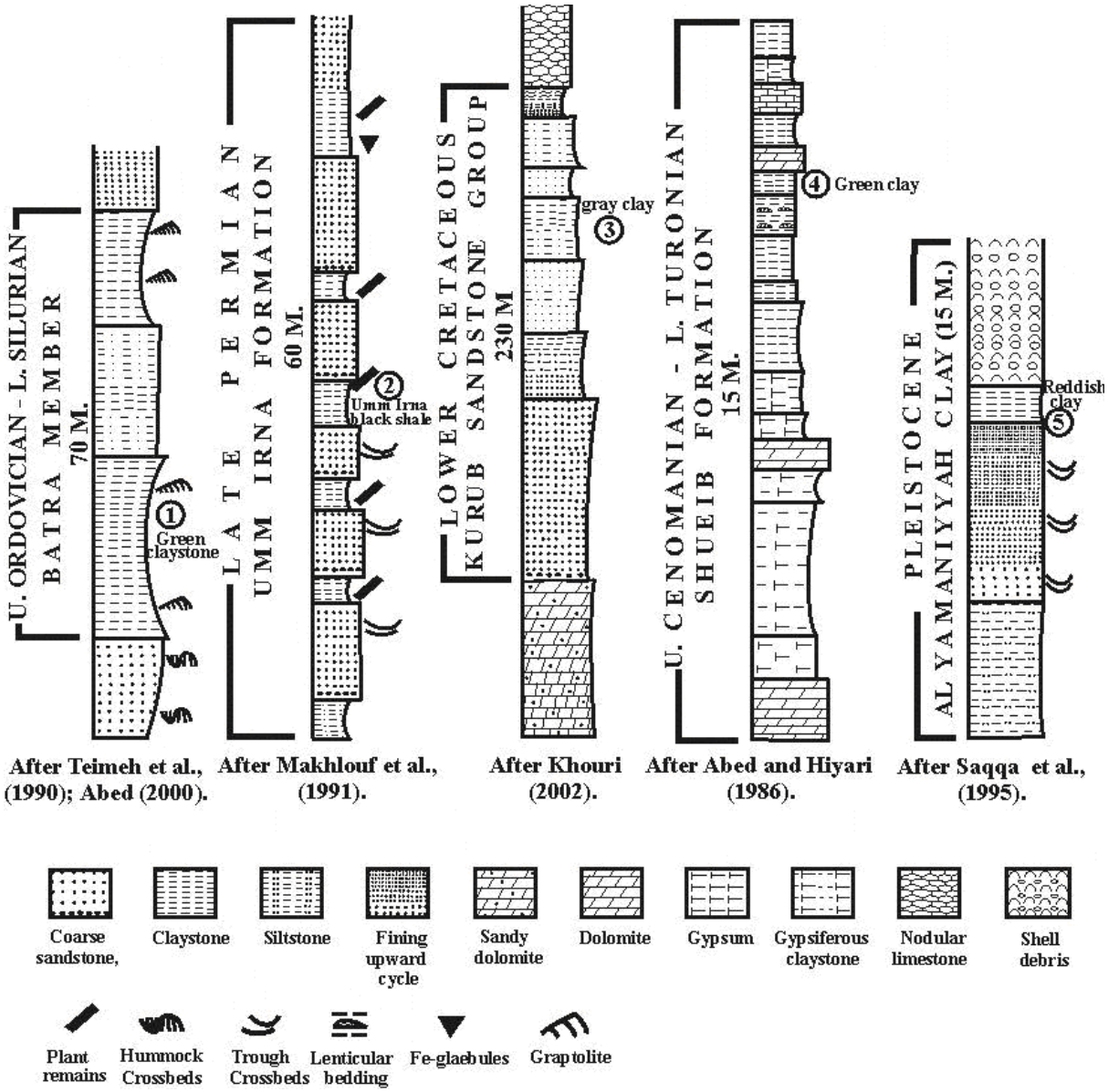

Fig.2. Generalized columunar sections from which mudrock samples were selected.
{(Reference samples denoted in text as :SIL (sample 1), UI(sample 2), MAH (sample 3), TAF(sample 5)}.

formation consists principally of dolomitized carbonate rocks and marl interbedded with gypsum layers of different textures with green and red-colored gypsiferous clay stone (Fig. 2). The fifth and the youngest sample (sample Ref., YAM) was selected from the upper red-brownish clay stone horizons of the Pleistocene Al-Yamaniyya clay deposits cropping out 6 km east of the Gulf of Aqaba, not far from Saudi borders with Jordan in the south. The varicolored claystone deposits interbedding sandstone of various sizes from course to fine (Fig.2) indicating a near shore environment (Ibrahim and Abdelhamid, 1990; Abu Halima, 1993; Saqqa et al., 1995).

3. Experimental

Mud rock samples were gently crushed, using an agate mortar and pestle. Samples were then treated only with 12% H_2O_2 to remove organic matter. Samples were wet sieved using a test sieve of 45µm to discard coarser fractions. The clay fraction (< 2 µm) was obtained from the pass 45 µ fraction by sedimentation, centrifuging and dialysis. The clay fraction (< 2 µm) was sedimented on a polished silicon-wafer substrate and left to dry at room temperature. After mounting, air-dried samples were heated at two different temperatures 350°C, 550°C. The samples were then ethylene glycolated at 60°C for 16 hours. PVP-10 (Polyvinylpyrrolidone) intercalated air-dried clays (< 2 µm fraction) were prepared, mounted on silicon-wafer substrates and analyzed by XRD for the purpose of measuring the fundamental illite particle thicknesses and their distributions (Eberl et al., 1998a).

In study samples, ratios of PVP to clay intercalations were as follows:

Sample	Ratio PVP : CLAY
YAM	4:1
TAF	3:1
MAH	2:1
UI	2:1
SIL	2:1

Clay fraction was suspended in distilled water (concentration 2.5mg clay/1ml H2O), then mixed with an aqueous solution containing 5mg PVP/1ml H2O fully dispersed by ultrasonic treatment. The proportion of clay to PVP used depended on the expandability of clay sample. The larger the proportion of smectite layers, the more PVP is added to obtain good intercalation. Samples presumed to have < 50% smectite content were mixed in proportions of 5 mg PVP to 2.5 mg clay (1 ml PVP solution/1 ml clay suspension), whereas the amount of PVP added for clays containing > 50% smectite was chosen by interpolation between former proportion, and that used for pure smectite (10 mg PVP to 2.5 mg clay or 2 ml PVP solution/1ml clay suspension). The mixtures were shaken by hand, left for a few minutes, sonified and then mounted appropriately for XRD scan (Dudek et al., 2002). The treatment with PVP-10 was applied for measuring sizes of illite particles. For kaolinite, such treatment was not required. The advantage of the PVP-10 intercalation is to remove the effect of peak broadening related to swelling interface of the exposed basal surfaces (containing H2O and exchangeable cations) of illite. In this way crystallite thicknesses could be calculated accurately by the BWA method. In the meantime the use of silicon wafers as substrates improved significantly the background of the XRD spectra (Eberl et al., 1998a; Drits et al., 1998; Bove et al., 2002). The 001 reflection of PVP-illite and kaolinite was measured by the BWA-method, using the MudMaster computer program (Eberl et al., 1996). The mean crystallite thickness, CTDs, the mean of natural logarithms of thicknessesα, and the variance of natural logarithms of thicknesses $\beta 2$ were all determined by applying the foregoing method. The measured CTDs were compared to theoretically calculated shapes of CTDs, using the GALOPER computer program (Eberl et al., 2000). The size of critical nucleus was set to 2nm when the modeling results were compared to BWA-PVP data in case of illite or to BWA data only in case of kaolinite. X-ray analysis was carried out using a Phillips PW1710 Diffractometer equipped with copper tube and a theta compensatory slit assembly. The system was operated under the following experimental conditions: a voltage of 35 kV, beam current of 40 mA, 2θ step size of 0.02º, counting time of 0.01 sec/step, 1 mm receiving slit and a scanning range of 2-65° 2θ. The BWA method adapted in the MudMaster computer program is based on Fourier analysis of the interference function (Eberl et al., 1996; Drits at al., 1998). The peak shape analysis for the purpose of measuring the mean crystallite thickness and the CTDs was for the 001 basal reflection of illite (I) and kaolinite (K).

4. RESULTS

a. XRD Analysis

The XRD patterns (Fig. 3; Table 1) show that illite (I) and kaolinite (K) are the main clay minerals in the Upper Ordovician–Lower Silurian Batra Member clay- stone (SIL sample). In the Late Permian Umm Irna black shale (UI sample) and in the Lower Cretaceous Mahis claystone (MAH sample) asymmetric broad mixed-layer illite-smectite (I-S) peaks of low intensity appear at 7.7° 2θ and 7.2° 2θ together with I and K. The mixed layer I-S peaks collapsed to 8.8° 2θ by heating at 550 °C. In the Lower Turonian Tafila green claystone (TAF sample), a broad peak of I/I-S appears around 8.02° 2θ in the air-dried X-ray pattern (Fig.3; Table 1). After ethylene glycolation, this peak was completely separated into two other peaks: one at 5.4° 2θ referring to Mg-smectite (S) and the second at 8.8° 2θ for illite. Środoń (1980) and Weibel (1999) considered the type of mixed layer I-S which completely separated into two peaks after ethylene glycol saturation as a random one. By heating at 550°C, smectite (S) in the mixed layer collapsed to the position of illite at 8.8° 2θ. Kaolinite (K) was also present in the Tafila claystone.

Mg-smectite (S) dominates other clay minerals in the Pleistocene Al-Yamaniyyah claystone (YAM sample). To a lesser extent is kaolinite (K), illite (I), mixed layer I-S, chlorite (Ch) and mixed layer illite-chlorite (I-Ch). The original *001* peak of smectite (S) at 6.2° 2θ in air-dried sample expanded to 5° 2θ after ethylene glycol saturation (see Fig.3; Table 1). The same peak collapsed upon heating at 550 °C to 9.04° 2θ (9.8X). The display of chlorite (Ch) and mixed layer illite-chlorite were verified after heating at 550 °C as shown in figure 3.

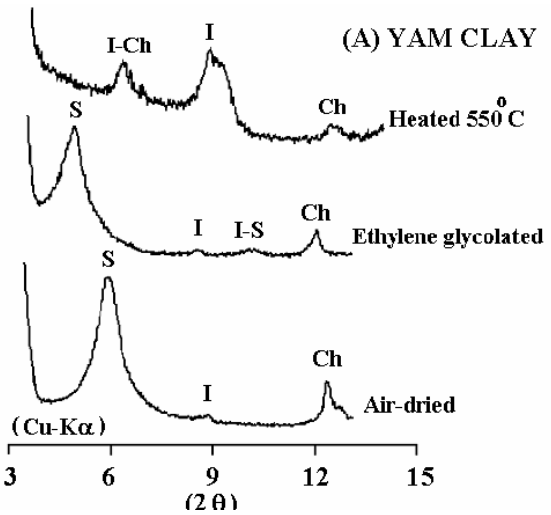

Fig.3 continues next page……

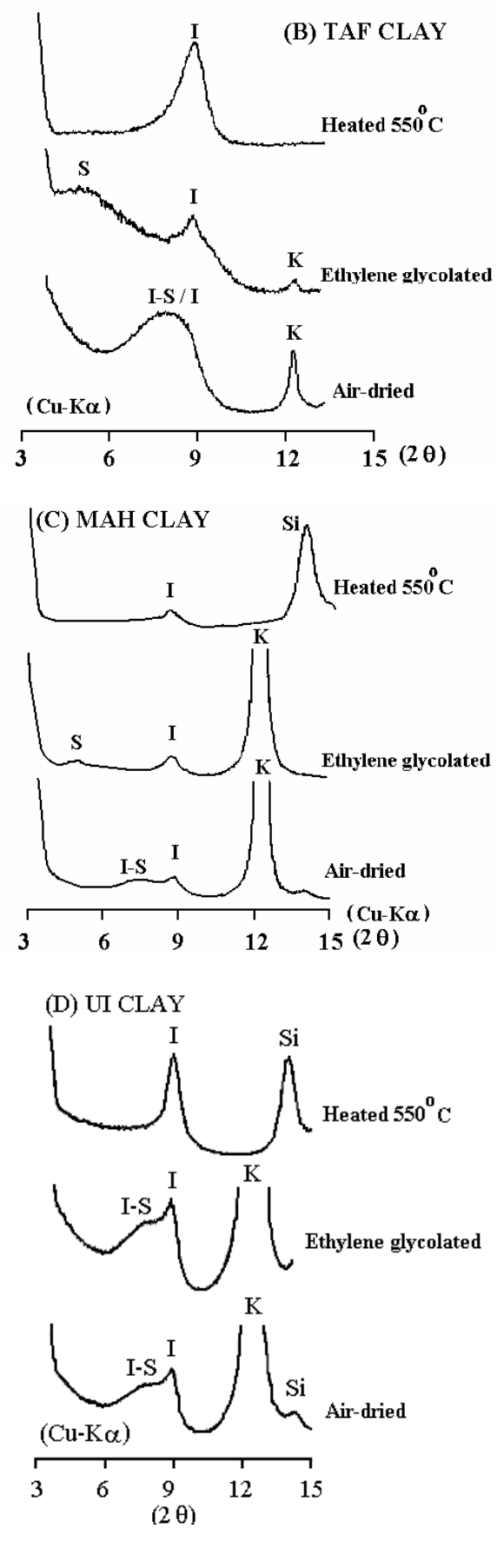

Fig. 3: X-ray diffractograms (air-dried, ethylene glycolated, heated at 550°C) of study samples.

S=Smectite, I-S= mixed layer illite-smectite, I=illite, K=Kaolinite, Ch =Chlorite, I-Ch= mixed layer illite-chlorite, Si=Silicon wafer.

b. Changes in particle size of illite and kaolinite with burial depths:

Table (2) summarizes results of mean particle thickness (T_{mean}), α, β2, CTDs shapes of illite (I) and kaolinite (K) with corresponding burial depths and temperatures. For illite (I) the mean particle thickness (T_{mean}) ranges from 2.8 nm - 3.3 nm. Although mean particle thickness (T_{mean}) of illite (I) shows no significant variations with depth, the natural conditions under which the relevant illite (I) formed are quite different.

For Kaolinite (K), the mean particle thickness (T_{mean}) slightly varies from one sample to another. They range in size from 3 nm-10.7 nm. At the beginning, slight increase in the mean particle thickness (T_{mean}) of kaolinite particles from 3 nm-3.7 nm resulted through a change in burial depth from a shallow depth to about 0.95 km. This is followed by a sharp increase from 3.7 nm-9.0 nm only within a small increase in burial depth of about 150 m. Again, a progressive increase in the mean crystallite thickness, 9.0 nm – 10.7 nm, was observed within a burial depth from 1.05 km-1.22 km. Beyond this depth, the mean particle thickness (T_{mean}) flipped toward a slight decrease with mean crystallite thickness difference of 0.7 nm as the burial depth approaches 1.6 km.

c. Crystallite thickness distributions (CTDs) for illite (I) and kaolinite (K):

The CTDs for PVP-illite (air dried samples) and kaolinite (heated at 350°C samples) were calculated as area-weighted in the BWA technique (Eberl, 1998b). Figure (4) illustrates the shapes of crystallite thickness distributions (CTDs) for illite (I). The CTDs of illite (I) in study samples are similar with asymptotic shapes indicating higher influence of simultaneous nucleation and growth except MAH sample which looks lognormal. Illite's T_{mean} is between 3.8 nm-5.2 nm). Figure (5) illustrates the CTDs shapes for kaolinite (K). They look

Table (1). Summary for XRD data between 3°-15 ° 2θ of all studied samples.

Name of Sample	Air-dried (2θ) d(Å)		Ethylene-glycolated (2θ) d (Å)		Heated (550°C) (2θ) d (Å)	Clay mineral
YAM	6.2 14.25	shifted to	5.0 17.67	collapsed to→	9.04 9.8	smectite
	n.d. n.d.	→	n.d. n.d.	→	6.54 13.5	illite-chlorite (Illite 30-40%).
	8.88 10	slightly increased to	8.68 10.10	slightly shifted to	9.04 9.8	illite
	n.d. n.d.	→	10.3 8.6	shifted to	9.04 9.8	illite-smectite (Illite 10%)
	12.42 7.13	→	12.2 7.25	→	12.62 7.02	chlorite
	12.48 7.09	→	12.34 7.17	→	destroyed	kaolinite
TAF	8.02 11.02	separated to two peaks:	1) 5.2 17.0 2) 8.8 10.0	1)collapsed to 2) unchanged	8.8 10.0 8.8 10.0	illite-smectite smectite illite
	12.32 7.18	unchanged	12.32 7.18	→	destroyed	kaolinite
MAH	6.92 12.7	separated to two peaks:	1) 5.4 16.3 2) 7.2 12.3	1)collapsed to 2) →	8.8 10.0 →	illite-smectite smectite illite-smectite
	8.8 10.0	slightly shifted to	9.04 9.78	unchanged	8.8 10	illite
	12.38 7.15	unchanged	12.38 7.15	→	destroyed	kaolinite
UI	7.7 11.5	unchanged	7.7 11.5	collapsed to	8.8 10	illite-smectite (illite 80%)
	8.94 9.89	unchanged	8.94 9.89	unchanged	8.94 9.89	illite
	12.4 7.13	unchanged	12.4 7.13	→	destroyed	kaolinite
SIL	8.92 9.91	v. little change	9.02 9.8	unchanged	8.92 9.91	illite
	12.44 7.12	unchanged	12.48 7.2	→	destroyed	kaolinite

asymptotic for both YAM and TAF samples, multimodal for MAH sample and lognormal for both UI and SIL samples. The distribution shapes indicate changes in crystal growth mechanisms from constant rate nucleation accompanied with growth (shallow-moderate depths) to a state of growth without continued nucleation at greater depths.

d. α versus β2 diagram

Illite CTDs were characterized further by simulating illite (I) crystal growth using the GALOPER computer program (Eberl et al., 2000). For this purpose the parameter α, the mean of the natural logarithms of thicknesses, was plotted versus the parameter β^2, the variance of the natural logarithms of thicknesses, together with theoretical paths of two crystal growth mechanisms. The first is the simultaneous nucleation and surface-controlled growth, and the second is the surface-controlled growth without nucleation (Eberl et al., 1998a; Środoń et al., 2000; Bove et al., 2002). In the first mechanism, new illite (I) nuclei continue to form at a constant rate while previously nucleated crystals continue to grow. During the second mechanism, growth occurs on previously nucleated crystals without new nucleation (Eberl, 1998a). Figure (6) shows that all asymptotic shapes of illite (I) are plotted close to the path line "AB" which reflects the first mechanism, i.e. simultaneous "constant rate" nucleation and surface-controlled growth. This crystal growth mechanism proceeds with constant rate nucleation of 2 nm thick-layered illite (I) which subsequently experiences size

Table (2): Parameters of mean crystallite thickness T_{mean} (best mean), $\propto$,β^2, d-spacing and CTDs shapes of PVP-illite and kaolinite as a function of burial depth and the corresponding temperature of all studied samples.

Sample	Burial depth (m)	Temperature (C°)	Best mean, T_{mean} (nm)	$\propto$	β^2	2θ	d-spacing (Å)	CTDs shape
YAM	shallow	surface T.	2.8	0.93	0.16	8.78	10.07	Asymptotic.
TAF	950	45	3	1.01	0.17	9	9.83	Asymptotic
MAH	1050	50	2.9	0.96	0.17	8.74	10.12	Asymptotic
U I	1220	58	3	0.99	0.18	8.82	10.03	Asymptotic.
SIL	1600	70	3.3	1.04	0.23	8.76	10.09	Asymptotic

B. Kaolinite (Heated at 350° samples)

Sample	Burial depth (m)	Temperature (C°)	Best mean T_{mean} (nm)	$\propto$	β^2	2θ	d-spacing (Å)	CTDs shape
YAM	shallow	surface T.	3	0.8	0.44	12.42	7.13	Asymptotic
TAF	950	45	3.7	0.81	0.75	12.34	7.17	Asymptotic
MAH	1050	50	8.9	2.07	0.66	12.34	7.17	Multimodal
U I	1220	58	10.7	2.25	0.29	12.42	7.13	Lognormal
SIL	1600	70	10	2.2	0.36	12.36	7.16	Lognormal

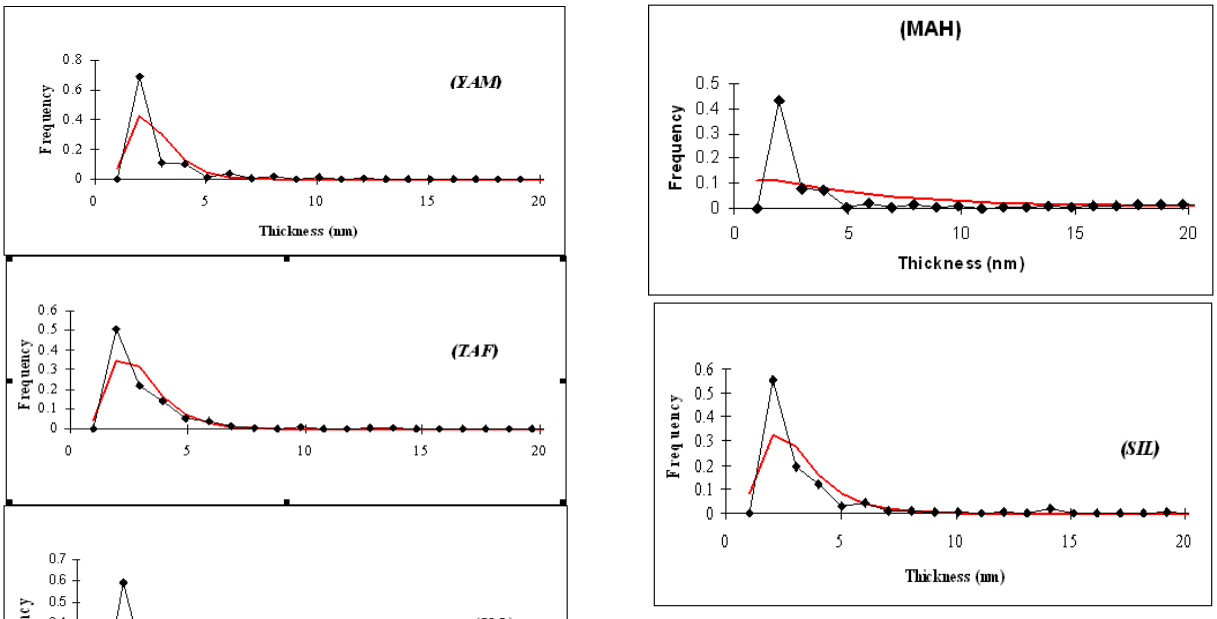

Fig. 4: Shapes of Illite particle thickness distributions in study samples using the BWA-PVP technique.

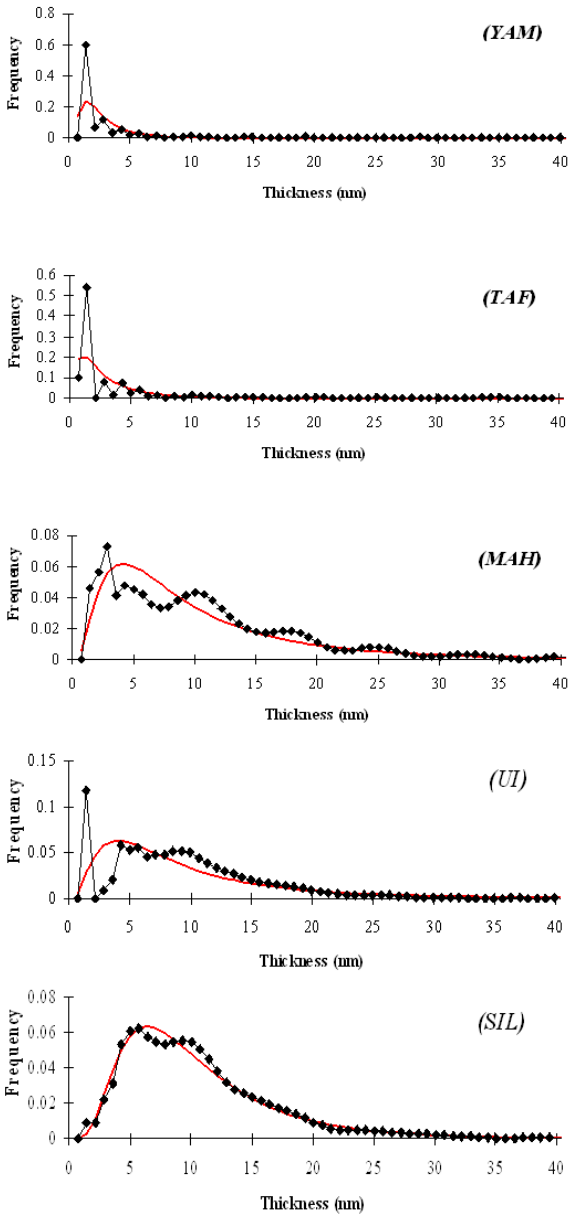

Fig. 5. Shapes of kaolinite particle thickness distributions in study samples using BWA-PVP technique.

dependent growth by the Law of Proportionate Effect "LPE" (Eberl et al., 1998a; Środoń et al., 2000; Bove et al., 2002). The asymptotic shapes of illite (I) to the left of the path line "1" could indicate that the final nucleation was not accompanied by growth.

5. Discussion

Results of raw X-ray data emphasize the fact that diagenetic changes in clay mineral types must take place through geological time. Smectite (S), which predominates other clay minerals in the Pleistocene Al-Yamaniyya surface clay deposits, is no longer abundant in the Turonian Shueib clays, Tafila area (TAF sample) and in the Lower Cretaceous Mahis clays (MAH sample), where the depth of burial approaches 1 km. Smectite (S) began to change into mixed layer I-S. Illite (I) and I-S are chief constituents in Tafila clays with subordinate kaolinite (K) and minor smectite (S). In the Lower Cretaceous Mahis clays kaolinite (K) predominates other clay minerals and illite (I) is less dominant. Progressive illitization was more likely enhanced after a burial depth of 1 km. Significant peaks of illite (I) and kaolinite (K) are typical in the late Permian black shale of Umm Irna Formation (UI sample) where the burial depth approximates 1200 m and in the Upper Ordovician-Lower Silurian green claystone of Batra Member of a burial depth 1600 m. Based on the obtained results, the distinct appearance of illite (I) peaks in the moderately to deeply buried Paleozoic clays indicates that this mineral was formed from diagenetic alterations of smectite (S) and S-I precursors. The degradation of smectite (S) and its transformation to illite (I) involve the incorporation of potassium (K+) ions into smectite structure and loss of interlayer water (Dunoyer de Segonzac, 1970; Hower et al., 1976). Compaction of mud through overburden pressure soon removes much of the water contained in lattices of clay mineral and water adsorbed onto clay surface or the less common pore filled water. At depths greater than one kilometer (temperature ≥ 45 °C), 70-90% of the original volume of water is reduced to about 30%. Further compaction through water loss requires temperature of about 100 °C. These are attained at greater depths (2-4 km). Dehydration of clays then takes place causing some changes in clay minerals types. Final compaction, leading to mudrock with only small percent water needs much longer period of overburden pressure with elevated temperature (Tucker, 1981, 1991). Amireh et al., (1994) studied the diagenesis in Paleozoic-Cretaceous sandstones in Jordan, pointed to the degradation of detrital muscovite into kaolinite and postdating of newly formed kaolinite to quartz overgrowth. They also observed the formation of dickite after kaolinite in the pore spaces of the Cambrian-early Ordovician sandstone (burial depth >2 km). Despite the significance of temperature and burial history as controlling parameters to diagenesis, we can't ignore the role of other controlling parameters such as tectonic uplift and sediment unroofing, which undoubtedly trigger sub aerial weathering for the unroofed sediments through geological time. Another criterion which may complicate the origin of clay minerals is the possible occurrence of the same types of clay minerals in more than one particular environment (terrestrial-marine) with different physical and chemical conditions. Therefore, in this work we attempted to give answers to questions raised about the origin of the investigated argillaceous rocks, giving the issue of primary origin of clay minerals great consideration.

The coexistence of kaolinite (K) and smectite (S) in the Pleistocene Al-Yamaniyya clays can only be explained on the basis of their primary origin after chemical weathering of the source materials. These two minerals very likely originated from a relatively high weathering of the very near Precambrian granitic source rocks intruded by mafic dikes. Weathering products were transported by streams draining granitic terrains and later deposited in a lacustrine environment separated from sea by some beach terraces (Abu Halimeh, 1993; Saqqa et al., 1995; Khouri, 2002). Leaching of iron and magnesium from weathering products leaves behind concentrations of silicon and aluminum to yield kaolinite crystals.

In the Lower Turonian Tafila clays, dolomite and gypsum interbed green and red claystone beds. The whole sediments were deposited in a coastal sabkha after tectonic uplift at the beginning of the Turonian age. The tectonic event caused sea level fall resulting in the development of the sabkha environment (Abed and El Hiyari, 1986). Tafila claystone were more likely deposited during periodic influxes of fresh water (e.g. Droste, 1963) at the time of sedimentation. After deposition, detritus clays were subjected to diagenetic changes, and new clay phases resulted through which smectite (S) altered to I-S and illite (I) under conditions of a saline lake or the sabkha. In most lake brines calcite or aragonite and/or gypsum precipitate early where Mg/Ca ratio is relatively low. The increase in Mg/Ca ratio causes Mg-rich minerals to precipitate such as dolomite, sepiolite and Mg-smectite (Weaver, 1989). Honty et al., (2004) noted that illitization of salt-bearing bentonite was enhanced by the aid of salinity and burial temperature. These authors referred to some studies that focused on the formation of I-S from smectite at surface conditions in sediments of saline lakes. Similarly, in their study, Turner and Fishman (1991) discussed illitization of smectite in altered tuff beds in a Jurassic lake with the absence of the effect of deep burial and lack of hydrothermal alteration. They concluded that solution chemistry was the principal factor controlling illitization of smectite at the surface temperatures. Eberl et al., (1986) realized that illitization of smectite is possible through wet-dry cycles. This is common in saline environments. In the presence of K+ ions, wet-dry cycles lead to irreversible fixation of K+ ions and formation of illite. Similarly, Stoffers and Singer (1979) described genesis of physils in Lake Albert sediments which reflected the evaporation history of its water. These authors believed that detrital smectite in bottom sediments were produced when the lake was open and the concentration of dissolved ions was low. I-S formed when the lake became closed and its water level was at its lowest. Ionic concentration increased and K+ content became high enough to start the process of illitization. With regard to the genesis of the green clays (TAF sample), we may suggest here that these clays were originally developed from the reduction of hematite in red clays by leaching of wet cycles at surface conditions. This idea can be supported by the absence of chlorite from the green clays (not detected in the X-ray data), which can impart green color for clays in nature. In addition to the above discussion about the genesis of green clays, we also believe that these clays were subjected to early diagenetic illitization as a result of surface wet-dry cycles, evaporation, and fixation of K+ ions. Absence of halite beds from the rock sequence of the Lower Turonian Shueib Formation (Tafila area) support the lack of NaCl concentrations from the depositional medium. This significantly enhances K+ ions fixation in clays (Honty et al., 2004). A burial depth of about one kilometer may help the transformation of smectite to mixed layer I-S.

Mahis clays (MAH sample) which are a part of fluvial system sediments (Abed, 1982; Khoury, 2002) have two origins, detrital (primary) and diagenetic. Some kaolinite produced from degradation of detrital feldspar and mica and some other kaolinite are authigenic. Khouri (2002) reported the presence of small authigenic kaolinite flakes adhered to quartz surfaces as a result of diagenesis after sedimentation. Intensive leaching of the detritus in acidic medium helps kaolinization process aided by rainfall and surface running water. Field observations confirmed the presence of carbonized plant remains in the gray clays of Mahis. The breakdown of plant remains and release of CO2 due to compaction caused the creation of acidic medium in the pore water. This initiated the neoformation of kaolinite (K) at depths surpass 1km (T>50 °C). The minor content of I-S and the initial presence of illite (I) suggest that more advanced stages of illitization were enhanced at the same depths.

Coalified plant remains were found also in the Late Permian Umm Irna black shale (UI sample). This again promoted the creation of acidic medium in the pore water as a result of organic matter decay and CO2 release possibly by thermal maturation at greater depths (> 1200 m). Accordingly, crystal growth of primary kaolinite (K) flakes took place. The strong appearance of illite and kaolinite peaks as viewed from the XRD analysis supports a continued smectite illitization and the increase of kaolinite crystallinity with burial depth.

The marine green clays (SIL sample) of the Upper Ordovician-Lower Silurian Batra Member are intercalated with fine sandstone and siltstone materials with an abundance of Graptolite remains at the bedding planes of green clays. After sedimentation, the compaction of sediments by the overlying rocks (burial depth >1.6 km) caused a set of physical and chemical changes to these sediments. Thus, illitization process proceeded and the crystallinity of kaolinite (K) was increased. This was despite the detrital origin of these clays which were derived from the older highly weathered underlying rocks.

MudMaster analyses showed that the distribution curves (CTDs shapes) of PVP-illite samples were all asymptotic attained at burial depths from a shallow depth to about 1.6 km. These results would explain the diagenetic origin of illite after a detrital source. As discussed earlier, the mechanism of illite crystal growth is expressed as a simultaneous nucleation together with growth where new illite nuclei continue to form at a constant rate while previously nucleated crystals continue to grow. An indication to illite crystals growth can be deduced from the Tmean increase obtained when the burial depth exceeded 1.05 km. Eberl (2004) found that the asymptotic shape of illite (I) can be related to sedimentation origin. It can also be obtained for illite (I) from analyzed shale samples and in a hydro thermally-altered wall rock. In the present work, there was no evidence for hydrothermal activities. Hence diagenesis postdating sedimentation process is most likely to be the reason for the asymptotic distribution form and the simultaneous nucleation and growth of illite crystals. This is regardless of the changes in temperature, pressure and time progress within the zone of diagenesis prior to arriving low grade metamorphism. However, the asymptotic CTDs shape also could be due to detrital illite. On the other hand, kaolinte CTDs shapes were asymptotic in the investigated younger sediments at burial depths of less than1km. This is followed by multimodal distribution at slightly deeper burial depth of 1.05 km. At relatively greater depths of 1.6 km, the distribution changed into lognormal form. The change in distribution forms might be interpreted on the basis of sedimentation and early

diagenesis of kaolinite (K) taking place at a burial depth of 1 kilometer and allowing for simultaneous crystals nucleation and growth. After this depth, kaolinite growth mechanism changed through an intermediate stage of a multimodal thickness distribution shape to lognormal shape at greater depths (>1.6 km) where nucleation ceased and growth only continued. This explanation of the change in CTDs shapes of kaolinite (K) from asymptotic to lognormal could be supported by the fact that the 00l kaolinite peaks are of high intensity, narrow and more symmetric reflecting well-ordered crystals in older deep buried sediments in comparison with more recent sediments buried at moderate-shallow depths.

6. Summary and Conclusions

The present work revealed that diagenetic changes of the identified clay minerals took place at various depths. Smectite (S) decreased and finally transformed into illite (I) through an intermediate mixed-layer I-S after exceeding a burial depth of one kilometer. Transformation of clay mineral species from primary into authigenic was produced under different depositional settings (terrestrial-marine). For instance, illitization process in the Lower Turonian Tafila green clays was enhanced in a saline sabkha environment by the aid of wet-dry cycles and K-ions fixation at surface conditions. This was aided by a tectonic uplift and unroofing of the Lower Turonian carbonate sediments of Shueib Formation. Deep burial was a crucial factor for illite crystallization and the increase of kaolinite crystallinity. Results obtained from MudMaster calculations were consistent with the observed X-ray diffraction data regarding illitization of smectite (S) and mixed layer I-S after sedimentation process. Simultaneous nucleation and continuous growth of illite nuclei interpreted from the asymptotic shape in all samples clearly reflect the effect of illitization of smectite into illite during burial history. The changes in CTD's of kaolinite (K) from asymptotic to lognormal through a multimodal phase reflect the variations in kaolinite crystal growth mechanisms with burial depth.

Acknowledgments

The authors would like to thank Dr. F. Ababneh of the Physics Department, Yarmouk University for operating the X-ray Diffractometer. For the anonymous referees, we extend our appreciation for their comments and critique.

References

[1] Abed, A. (1982). Depositional environments of the Early Cretaceous Kurnub (Hathira) Sandstones, North Jordan. Sedimentary Geology, **31,** 267-271.

[2] Abed, A. and El-Hiyari, M. (1986). Depositional Environments and Paleogeography of the Cretaceous gypsum horizon in west-central Jordan. Sedimentary Geology, **47**, 109-123.

[3] Abed, A. (2000). Geology, Environment and water of Jordan (in Arabic). Published by Jordanian Geological Association, Scientific Books Series 1, Amman, 571pp.

[4] Abu Halima, K. (1993). Mineralogy, chemistry and industrial studies of Al-Yamaniyya clay deposits in Aqaba area. M.Sc. thesis, University of Jordan, Amman.

[5] Amireh, B.S., Schneider, W. and Abed, A.M. (1994). Diagenesis and burial history of the Cambrian-Cretaceous sandstone series in Jordan. *Neues Jahrbuch für Geologie und* Paläontologie Abhandlungen **192**,151-181.

[6] Árkai, P., Merriman, R.J., Roberts, B., Peacor, D.R. and Tóth, M. (1996). Crystallinity, crystallite size and lattice strain of illite-muscovite and chlorite: comparison of XRD and TEM data for diagenetic to epizonal pelites. European Journal of Mineralogy **8**, 1119-1138.

[7] Langford, 1978

[8] Bove, D.J., Eberl, D.D., McCarty, D.K. and Meeker, G.P. (2002). Characterization and modeling of illite crystal particles and growth of mechanisms in a zoned hydrothermal deposit, Lake City, Colorado. American Mineralogist **87**, 1546-1556.

[9] Brime, C. and Eberl, D.D. (2002). Growth mechanisms of low-grade illites based on the shapes of crystal thickness distributions. Schweizerische Mineralogische und Petrogrphische Mitteilungen **82**, 203-209.

[10] Brindley, G.W., Brown, G. (1980). Crystal structures of clay minerals and their X-ray identification. Mineralogical Society, London, 495pp.

[11] Drits, V., Środoń, J. and Eberl, D.D. (1997). XRD measurement of mean crystallite thickness of illite and illite/smectite: reappraisal of the Kübler index and the Scherrer equation. Clays and Clay Minerals **45**, 461-475.

[12] Drits, V., Eberl, D.D. and Środoń, J. (1998). XRD measurement of mean thickness, thickness distribution and strain for illite and illite/smectite crystallites by the Bertaut-Warren-Averbach technique. Clays and Clay Minerals **46**, 38-50.

[13] Droste, J.B. (1963). Clay mineral composition of evaportie sequences. Northern Ohio Geological Societ*y* **1**, 47-54.

[14] Dudek, T., Środoń, J., Eberl, D.D., Elsass, F. and Uhlik, P. (2002). Thickness distribution of illite crystals in shales. Part 1: X-ray diffraction *vs*. high-resolution transmission electron microscopy measurements. Clays and Clay Minerals **50**, 562-577.

[15] Dunoyer de Segonzac, G. (1970). The transformation of clay minerals during diagenesis and low grade metamorphism: a review. Sedimentology, **15**, 281-346.

[16] Eberl, D.D., Środoń, J. and Northrop, H.R. (1986). Potassium fixation in smectite by wetting and drying. In Geochemical Processes at Mineral Surfaces (Davis and Hayes, editors), ACS Symposium Series, 323, American Chemical Society.

[17] Eberl, D.D. and Velde, B. (1989). Beyond the Kübler index. Clay and Clay Minerals **24**, 571-577.

[18] Eberl, D.D., Drits, V.A., Środoń, J. and Nüsch, R. (1996). MudMaster: a program for calculating crystallite size distribution and strain from the shapes of X-ray diffraction peaks. U.S. Geological Survey, Open-File Report 96-171.

[19] Eberl, D.D., Drits, V.A. and Środoń, J. (1998a). Deducing growth mechanisms for minerals from the shapes of crystal size distributions. American Journal of Science **298**, 499-533.

[20] Eberl, D.D., Nüsch, R. Šucha,V. and Tsipursky, S. (1998b). Measurement of illite particle thicknesses by X-ray diffraction using PVP-10 intercalation. Clays and Clay Minerals **46**, 89-97.

[21] Eberl, D.D., Drits V.A., Środoń, J. (2000). User's guide to GALOPER- a program for simulating the shapes of crystal size distribution- and associated programs.

[22] U.S. Geological Survey Open File Report 00-505, 44pp.

[23] Eberl, D.D. (2004). Quantitative mineralogy of the Yukon River system: variations with reach and season, and determining sediment provenance. American Mineralogist, **89**, 1784-1794.

[24] Honty, M., Uhlik, P., Šucha, V., Čaplovičová, Franců, J., Clauer, N. and

[25] Biroň, A. (2004). Smectite-to-illite alteration in salt-bearing bentonites (The East Slovak Basin). Clays and Clay Minerals **52**, 533-551.

[26] Hower, J., Elsinger, E.V., Hower, M.E., Perry, E.A. (1976). Mechanism of burial metamorphism of argillaceous sediment: 1. Mineralogical and chemical evidence. Bulletin of Geological Society of America*,* **87**, 725-737.

[27] Ibrahim, K. and Abdelhamid, G. (1990). Al-Yamaniyya clay deposits. Internal Report, Natural Resources Authority, Amman.

[28] Jaboyedoff, M., Bussy, F., Kübler, B. and Thelin, Ph. (2001). Illite "crystallinity" revisited. Clays and Clay Minerals **49**, 156-167.

[29] Khouri, H.N. (2002). Clays and Clay Minerals in Jordan. Published by University of Jordan, Amman, 116p.

[30] J. I. Langford, A rapid method for analyzing the breadths of diffraction and spectral lines using the Voigt function, J. Appl. Cryst. (1978). 11, 10-14.

[31] Lanson, B., Beaufort, D., Berger, G., Baradat, J. and Lacharpagne, J.C. (1996). Late stage diagenesis of clay minerals in porous rocks : Lower Permian Rotliegendes reservoir off-shore of the Netherlands. Journal of Sedimentary Research **66**, 501-518.

[32] Makhlouf, I., Turner, B. and Abed, A.M. (1991). Depositional facies and environments in the Permian Umm Irna Formation, Dead Sea area, Jordan. Sedimentary Geology **73**, 117-139.

[33] Merriman, R.J., Roberts, B and Peacor, D.R. (1990). A transmission electron microscope study of white mica crystallite size distribution in a mudstone to slate transitional sequence, North Wales, UK. Contributions to Mineralogy and Petrology **106**, 27-40.

[34] Nieto, F. and Sánchez-Navaz, A. (1994). A comparative XRD and TEM study of the physical meaning of the white mica "crystallinity" index. European Journal of Mineralogy **6**, 611-621.

[35] Saqqa, W.A., Dwairi, I.M. and Akhal, H.M. (1995). Sedimentology,mineralogical evaluation and industrial applications of the Pleistocene Al-Yamaniyyah clay deposits, near 'Aqaba, southern Jordan. Applied Clay Science, **9**, 443-458.

[36] Środoń, J. (1980). Precise identification of illite/smectite interstratifications by X-ray powder diffraction. Clays and Clay Minerals **28**, 401-411.

[37] Środoń, J., Eberl, D.D. and Drits, V.A. (2000). Evolution of fundamental particle size during illitization of smectite and implications for reactions mechanism. Clays and Clay Minerals, **48**, 446-458.

[38] Stoffers, P. and Singer, A. (1979). Clay minerals in Lake Mobuto Seso Seko (Lake Albert) – their diagenetic changes as an indicator of the paleoclimate. Geologische Rundschau, **68**, 1009-1024.

[39] Teimeh M., Taani Y., Abu Lihie O. & Abu Saad L. (1990).- A study of the Palaeozoic formations of Jordan at outcrop and in the subsurface including measured sections and regional isopach maps.- Natural Resources Authority, Geology Directorate, Subsurface Geology Division, Bulletin*,* Amman, 1, p. 1–72.

[40] Tucker, M. (1981). Sedimentary Petrology an introduction. Blackwell Scientific Publications, Oxford, 252pp.

[41] Tucker, M. (1991). Sedimentary Petrology an introduction to the origin of sedimentary rocks. 2nd edition, Blackwell Scientific Publications LTD, Oxford, 260pp.

[42] Turner, C.E. and Fishman, N.S. (1991). Jurassic Lake T'oo'dichi': a large alkaline saline lake, Morrison Formation, eastern Colorado Plateau. Geological Society of America Bulletin **103**, 538-558.

[43] Weaver, Ch. E. (1989). Clays, Muds and Shales. Development in Sedimentology, **44,** Elsevier, Amsterdam, 819pp.

[44] Weibel, R. (1999). Effects of burial on the clay assemblages in the Triassic Skagerrak Formation, Denmark. Clay Minerals, **34**, 619-635.